Predicting Long Bone Loading From Cross-Sectional Geometry

Daniel E. Lieberman,[1]* John D. Polk,[1] and Brigitte Demes[2]

[1]*Department of Anthropology, Peabody Museum, Harvard University, Cambridge, Massachusetts 02138*
[2]*Department of Anatomical Sciences, Stony Brook University, Stony Brook, New York 11794-8081*

KEY WORDS second moment of area; cross-sectional geometry; in vivo strain; sheep; functional morphology

ABSTRACT Long bone loading histories are commonly evaluated using a beam model by calculating cross-sectional second moments of areas (SMAs). Without in vivo strain data, SMA analyses commonly make two explicit or implicit assumptions. First, while it has long been known that axial compression superimposed on bending shifts neutral axes away from cross-sectional area centroids, most analyses assume that cross-sectional properties calculated through the area centroid approximate cross-sectional strength. Second, the orientation of maximum bending rigidity is often assumed to reflect the orientation of peak or habitual bending forces the bone experiences. These assumptions are tested in sheep in which rosette strain gauges mounted at three locations around the tibia and metatarsal midshafts measured in vivo strains during treadmill running at 1.5 m/sec. Calculated normal strain distributions confirm that the neutral axis of bending does not run through the midshaft centroid. In these animals, orientations of the principal centroidal axes around which maximum SMAs (I_{max}) are calculated are not in the same planes in which the bones experienced bending. Cross-sectional properties calculated using centroidal axes have substantial differences in magnitude (up to 55%) but high correlations in pattern compared to cross-sectional properties calculated around experimentally determined neutral axes. Thus interindividual comparisons of cross-sectional properties calculated from centroidal axes may be useful in terms of pattern, but are subject to high errors in terms of absolute values. In addition, cross-sectional properties do not necessarily provide reliable data on the orientations of loads to which bones are subjected. Am J Phys Anthropol 123:156–171, 2004.

For many years, cross-sectional geometrical properties have been used to test hypotheses and make inferences about the mechanical adaptations of long bones. Many early studies of long bones examined cross-sectional area (CSA), which reflects a bone's resistance to axial compression and tension. More recently, second moments of area (SMAs, also termed area moments of inertia) were used preferentially in analyses of cross-sectional geometry because they better characterize the resistance of a long bone to bending around a particular axis (Wainright et al., 1976). Measures of CSA or bone thickness can provide poor estimates of strength to non-axial loading because resistance to bending depends on the distribution of area in a cross section. SMA (designated I) measures how material is distributed about a defined axis as:

$$I = \int_{-y_{max}}^{+y_{max}} y^2 \, dA$$

where A is area and y is the perpendicular distance to an axis through the centroid. In nonintegral form, I can be approximated by dividing a section into many squares of dimension x^2, each located a distance, y, from the neutral axis of bending (NA) (Fig. 1):

$$I = \sum_{i}^{n} x_i^2 \cdot y_i^2$$

Typically, I is calculated with respect to orthogonal axes defined by anatomical or arbitrary reference planes (I_{xx}, I_{yy}), or I may be calculated with respect to orthogonal principal axes (I_{max}, I_{min}). I, in turn, permits one to calculate the section modulus, Z, defined as $I \bullet (D \bullet 0.5)^{-1}$, where D is the section's diameter in the plane of bending. Z best approximates a cross section's resistance to bending in a given plane (Wainright et al., 1976). Polar moments

Grant sponsor: NSF; Grant number: IBN 96-03833.

*Correspondence to: Daniel E. Lieberman, Department of Anthropology, Peabody Museum, Harvard University, Cambridge, MA 02138.

Received 30 September 2002; accepted 22 March 2003.

DOI 10.1002/ajpa.10316
Published online 10 June 2003 in Wiley InterScience (www.interscience.wiley.com).

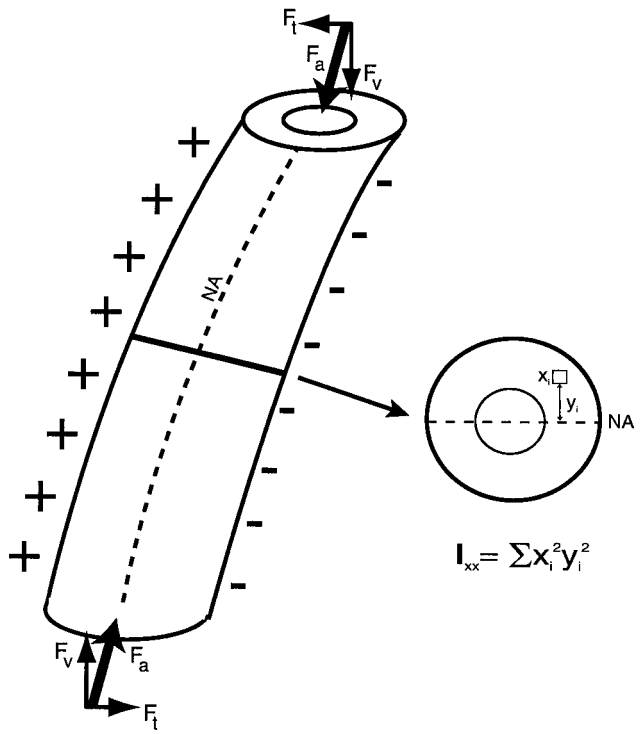

Fig. 1. Idealized cylindrical beam subject to loading at proximal end from body mass and at distal end from ground reaction force. Axial forces (F_a), which generate compression, can be resolved into transverse (F_t) and vertical (F_v) components. NA, neutral axis around which compressive (+) and tensile (−) strains occur. Bending moment at midshaft cross section is counteracted by second moment of area, I. See text for further details.

of area (or polar second moments of inertia), J, are calculated as the sum of any two perpendicular measures of I (e.g., $I_{xx} + I_{yy}$ or $I_{max} + I_{min}$); J describes both resistance to torsion of circular cross sections (Wainright et al., 1976; Carter and Beaupré, 2001; Daegling, 2002) and average bending rigidity (Schaffler et al., 1985). In addition, ratios of orthogonal SMAs ($I_{xx} \bullet I_{yy}^{-1}$ or $I_{max} \bullet I_{min}^{-1}$) were hypothesized to be useful quantifiers of cross-sectional shape, potentially providing information on the type of loading to which a bone is adapted and/or subjected (Lovejoy et al., 1976; Ruff and Hayes, 1983).

Limb bone cross-sectional properties have widely been used to make inferences about long bone adaptations in all sorts of vertebrates (e.g., Alexander, 1983; Selker and Carter, 1989; Biknevicius, 1993; Heinrich and Rose 1997; Cubo and Casinos, 1998; Heinrich et al., 1999), including comparisons between human populations (e.g., Ruff and Hayes, 1983; Ruff and Larsen, 1990; Ruff, 1992; van der Meulen et al., 1993; Bridges et al., 2000; Stock and Pfeiffer, 2001), between hominid species (Trinkaus, 1997; Trinkaus and Churchill, 1999; Trinkaus and Ruff, 1999; Trinkaus et al., 1999; Churchill and Smith, 2000), and between primate species (e.g., Schaffler et al., 1985; Ruff, 1987; Burr et al., 1989; Demes and Jungers, 1989, 1993; Demes et al., 1991; Ruff and Runestad, 1992; Ohman, 1993; Jungers and Burr, 1994; Terranova, 1995; Runestad, 1997; Jungers et al., 1998; Polk et al., 2000; Llorens et al., 2001; Kimura, 2002). In such comparisons, cross-sectional properties standardized by body mass and/or element length or dimensionless ratios such as $I_{max} \bullet I_{min}^{-1}$ provided important insights about loading history and locomotor adaptations. For example, it was long thought that Neanderthals had more robust bones than modern humans (e.g., Trinkaus, 1992). However, more recent analyses that plotted cross-sectional properties against tibial and femoral lengths adjusted for body mass and shape (for details of this adjustment, see Ruff et al., 1993; Trinkaus, 1997) found no significant difference in adjusted J between Neanderthals and early "anatomically modern" humans from the Near East, but significant differences in cross-sectional shape ($I_{xx} \bullet I_{yy}^{-1}$) (Trinkaus et al., 1998a, b; Trinkaus and Ruff, 1999). As a result, these authors concluded that Neanderthals and early "anatomically modern" modern humans had similar magnitudes but possibly different patterns of locomotor loading.

Several factors, however, complicate the use of cross-sectional properties for testing hypotheses about bone function or loading history. Most importantly, calculating cross-sectional properties from bone midshafts requires one either to determine experimentally or to make some assumptions about how a bone is bent during loading, using a beam model. Beams are defined as structural elements with fairly straight long axes whose length is several times greater than their width and depth. In general, long bones are typically modeled as solid or hollow cylindrical beams subjected to two-point bending by forces applied to their ends, as seen in Figure 1. Under such conditions, bending stress/strain at any location is a function of the magnitude and orientation of the two forces and the cross-sectional and material properties of the bone. For example, limb bones are often modeled at midstance, when ground reaction forces (GRFs) are high and approximately vertical. Elements not aligned with the GRF will be bent so that anterior and posterior cortices will experience compression or tension, respectively, depending on whether the GRF passes in front of or behind the element. In the case of the typical quadruped leg, illustrated in Figure 2A, the cranial (anterior) cortex of the metatarsal is predicted to be in compression, and the cranial cortex of the tibia is predicted to be in tension. Note also that more angled elements such as the tibia should experience greater bending stresses/strains because the moment arm to the GRF is longer (Biewener et al., 1983).

If a long bone is loaded in pure bending, then the neutral axis of bending will run through the area centroid of the shaft section (Wainright et al., 1976). However, it has long been appreciated that long bones are loaded by a combination of bending moments and axial forces (e.g., Pauwels, 1948; Lovejoy et al., 1976). Under such conditions, the neutral axis

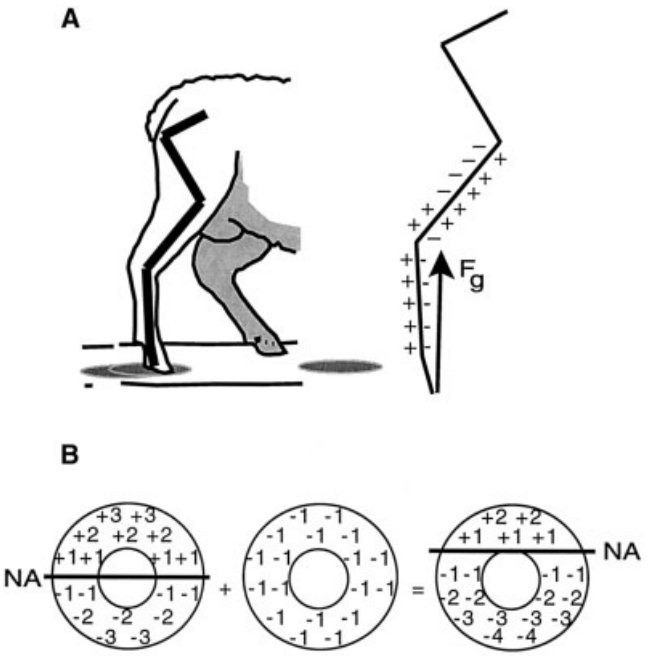

Fig. 2. **A:** Schematic view of sheep hindlimb at midstance. At right, approximate orientation of ground reaction force (F_g), relative to orientation of metatarsal and tibia. Cranial (anterior) cortex of metatarsal is predicted to be compressed. Bending in tibia depends on where it intersects with F_g (i.e., cranial part of proximal shaft should be tensed). **B:** Effect of axial compression on neutral axis position. At left, a section subject to pure bending, with hypothetical values of tension (positive) and compression (negative). Superimposition of an evenly distributed compressive force of −1, causes neutral axis (NA) to shift towards cortex, subject to tension.

will not pass through the centroid; instead, the superimposition of bending and axial compression shifts the neutral axis (NA) of bending away from the centroidal axis (CA) towards the cortex under tension, as illustrated in Figure 2B. Such shifts of the NA were demonstrated experimentally in the few published studies in which strain gauges were applied to at least three locations around a bone midshaft to solve the location of the neutral axis (Carter et al., 1981; Szivek et al., 1992; Gross et al., 1992; Judex et al., 1997; Demes et al., 1998, 2001). In addition, a few experiments bonded strain gauges to metal plates affixed to long bones (Carter et al., 1981; Gautier et al., 2000), with similar results. Unfortunately, such experiments are difficult to perform on most bones in most species, because the application of three gauges around a bone midshaft is liable to affect muscle function adversely, causing lameness or other abnormal kinematic and kinetic patterns. In addition, no such data are available for humans because, so far, the only way to estimate NA position is to apply strain gauges in vivo.

In the absence of experimental data on NA position (as is the case for all human studies), most researchers calculated cross-sectional geometric properties using the area centroid. This approach requires the assumption (sometimes explicit, but usually implicit) that there is a predictable, reliable relationship between cross-sectional geometric properties calculated around the CA vs. those calculated around the NA. Most analyses of cross-sectional geometry do not assume the *absolute* values of cross-sectional geometric properties to be correct, but the *relative* values or *patterns* of cross-sectional geometric properties are assumed to be useful if not approximately correct for making comparisons between individuals or species. This assumption has mostly been made for J, which, as the sum of any two orthogonal measures of I, "provides an indication of overall biomechanical structural integrity" (Trinkaus, 1997, p. 13,368). However, this assumption has never been tested by calculating cross-sectional geometric properties using experimentally determined neutral axes.

A second major problem is the relationship between form and function in the midshaft. In order to make inferences about loading history or structural adaptations in bones using cross-sectional properties, there has to be some predictable relationship between the orientation of bending in a bone and the distribution of area within the cross section. While J is often considered to be a general indicator of bending strength (see above), interpretations of other cross-sectional geometric parameters (notably I_{max}, I_{min}, and Z) are potentially more problematic. In particular, since I_{max} indicates the relative magnitude of greatest bending rigidity in a section, it has been considered reasonable to hypothesize that the orientation of bending is approximated by I_{max}. As stated by Ruff and Hayes (1983, p. 379), "Bone area appears to be distributed in such a way as to minimize stresses and strains developed under loading." However, experimental studies of limb shaft biomechanics yielded a confusing picture of the relationship between midshaft shape and cross-sectional distribution of strains. The analysis by Szivek et al. (1992) of femoral strain in the greyhound showed that the orientation of the NA was nearly anteroposterior at 0.6 m/sec (a slow walk), but rotated to 45° relative to a mediolateral axis at 1.2 m/sec (a slow trot), and to within 15° relative to a mediolateral axis at 2.4 m/sec (a moderate trot), when strains were higher. Gross et al. (1992) showed that the mediolateral orientation of the NA in the horse third metacarpal bone indicates anteroposterior bending at 3.6 m/sec (a moderate trot), even though the wide shape of the third metacarpal midshaft is clearly strongest to withstand mediolateral bending. Similarly, in studies by Demes et al. (1998, 2001) of the macaque tibia and ulna, the orientations of the NA differed substantially from I_{max} in both walking and galloping. At a walk, the macaque tibia was bent obliquely between 30–45° relative to I_{max}, and the macaque ulna was bent mediolaterally, approximately 90° relative to I_{max}. At higher speeds (a gallop), the NA of the tibia became more mediolaterally oriented (by about 20°). Thus, the extent to which loading patterns can be inferred from bone cross-sectional shape is not clear. Previous researchers

who noted the differences between cross-sectional bone shape and loading, mostly in distal elements, suggested that seemingly nonoptimal cross-sectional shapes are adaptations to increase the predictability of loads at the expense of strength (Lanyon and Rubin, 1985; Bertram and Biewener, 1988). However, with the exception of Demes et al. (2001), none of these studies explicitly tested the relationship between the orientations of NA and I_{max}.

Finally, dynamic changes in loads applied to bones during the stance phase at different speeds or gaits could further complicate the relationship between cross-sectional geometric properties and how bone shafts are bent (Biewener et al., 1988). Most of the experimental studies cited above, that calculated cross-sectional gradients using in vivo strain data, examined just midstance, when peak strains are typically highest. Only a few studies looked at dynamic changes through gait, with slightly different results. Demes et al. (1998, 2001) found no major change in how the macaque ulna and tibia were bent during the stance phase. Szivek et al. (1992) found little change in the orientation of NA in the dog femur between midstance and toe-off, but about 15° rotation between paw strike and midstance. Thus additional evidence is needed to characterize how bending regimes change during the stance phase. To complicate matters, midstance loading patterns sometimes differ by speed and gait. As noted above, Szivek et al. (1992) found more anteroposterior bending in the dog femur at higher speeds. Thus the shape of the dog femoral midshaft appears to reflect the orientation of forces applied to the bone at higher speeds. Demes et al. (2001), however, showed that the orientation of bending in the tibia, but not the ulna, in macaques shifted to a more anteroposterior pattern of bending between walking and galloping.

The above problems raise several questions about the relationship between bone cross-sectional shape and how bone shafts are loaded. First, to what extent is the direction of bending determined by bone shape, by local muscles forces, or by the ground reaction force and its position relative to the shaft? While in vivo strain data offer some support for the hypothesis that ground reaction force orientation relative to limb orientation is the primary determinant of bending orientation (Biewener, 1982, 1983; Biewener et al., 1983), these data were experimentally determined for only a few animals and limbs, and obviously cannot be known for extinct species. In addition, using the ground reaction force vector projected up the limb to assess bending moments is a method prone to error, especially for more proximal segments, where the discrepancy between the ground reaction force moment and the actual joint moment applied to the bone can be considerable (Wells, 1981; Winter, 1990). A second question is, how much do muscle and tendon forces influence patterns of bone loading? One in vitro study suggests that muscles and tendons may have some effects on overall bone loading (Peterman et al., 2001), and several experimental studies show that muscles contribute substantially to local stresses and strains (Barnes and Pinder, 1974; Biewener et al., 1992; Dial and Biewener, 1993). But more research is needed to test the effects of muscle forces on midshaft strains. Such forces, for example, were modeled but not tested in vivo with respect to gluteal abductor forces on the shaft of the femoral neck (Lovejoy et al., 1973; Ruff, 1995). And finally, what is the relationship between bone loading and midshaft shape? Application of Wolff's law to cross-sectional geometry was experimentally tested only partially (see also Biewener et al., 1986; Ruff et al., 1993, 1994; Lieberman, 1996; Qin et al., 1998; Goodship and Cunningham, 2001; Lieberman and Pearson, 2001; Rubin et al., 2001), and requires more research to examine the interactions of loading parameters, age, and skeletal location on phenotypic plasticity of cross-sectional geometry. While many studies showed that loading can stimulate growth (for a review, see Martin et al., 1999; but see also Bertram and Swartz, 1991), few experiments directly related orientations of experimentally measured bending to patterns of growth. Judex et al. (1997) found that rates of periosteal growth in the tarsometatarsus of adult roosters (which was mostly bent anteroposteriorly) correlated poorly with sites of peak strain magnitude. In contrast, Gross et al. (1997) found a rough correspondence between sites of peak compression and sites of peak bone growth in turkey radii that were functionally isolated and then artificially loaded. More studies are needed to evaluate growth changes in cross-sectional geometric properties in relation to experimentally determined midshaft cross-sectional strains.

HYPOTHESES TO BE TESTED

As noted above, many problems remain to be addressed in order to improve our understanding of the relationships between bone cross-sectional shape, bone function, and bone loading history. We focus here on the relationship between patterns of loading and cross-sectional geometry by using rosette strain gauges mounted at three sites around the midshaft of the tibia and metatarsal in juvenile sheep. By solving for the magnitude of strain normal to the long axis of the midshaft (see below) from each strain gauge, the position of the neutral axis and the cross-sectional distribution of tensile and compressive strains can be calculated based on simple beam bending theory (Rybicki and Mills, 1977). By analyzing the cross-sectional geometry of the same midshafts, we tested three hypotheses. First, while it has long been appreciated that the NA does not necessarily run through the area centroid of a midshaft, it was commonly assumed either explicitly or implicitly that measurements of cross-sectional geometric properties calculated using centroidal axes approximate, either in pattern or magnitude, cross-

sectional geometric properties that are calculated through an experimentally determined NA. We therefore tested the hypothesis that cross-sectional geometric properties calculated around an experimentally determined NA are equal to or approximate those calculated through the CA. Second, it is commonly assumed (sometimes explicitly but often implicitly) that the distribution of area in a midshaft cross section is related to the pattern of loading to which the bone is subjected. We therefore tested the hypothesis that the NA coincides in its orientation with the principal, centroidal axis of the cross section (CA_{max}, the axis around which the cross section offers greatest resistance to bending). Third, there are conflicting studies of the relationship between the distribution of peak strains in the midshaft and the dynamic changes in bending that occur throughout stance. We therefore tested the hypothesis that the orientation and position of the NA during the stance phase are stable and similar to its position at midstance.

In addition to these hypotheses, we also attempted to explore the statistical relationship between cross-sectional geometric parameters (I, J, and Z) calculated using CAs vs. NAs by extrapolating the results of in vivo strain gauge analyses to cross-sectional geometric properties in a large sample of sheep that were exercised on a treadmill for 3 months at the same speed for which we measured strains.

MATERIALS AND METHODS

Subjects

Dorset sheep (*Ovis aries*) were used for this experiment because they are docile, good treadmill runners, and have relatively little muscle mass on the tibia and metatarsal, permitting application of strain gauges at multiple sites without impairing normal gait. Strain gauges were applied to 5 juvenile sheep, all between 20–30 kg, who were trained to run at speeds up to 3 m/sec on a treadmill. Data presented here are for strains obtained at 1.5 m/sec (a moderate trot). For comparison, we also examined data on cross-sectional properties, element lengths, and body mass from Dorset sheep from three age categories: juvenile (aged 110 days, n = 10), subadult (aged 355 days, n = 10), and young adult (aged 505 days, n = 16); half of these sheep had been exercised daily for 90 days at approximately 1.5 m/sec (for additional details of this sample, see Lieberman et al., 2001).

Strain data acquisition

Prior to surgery, animals used in strain gauge experiments were sedated with ketamine (8.0 mg/kg, i.m.), xylazine (0.05 mg/kg, i.m.), and atropine (0.05 mg/kg, i.m.), intubated, and maintained on a surgical plane of anesthesia with isoflurane. The left hindlimb of each animal was shaved and sterilized, and the location of the midshaft was marked. Under sterile surgical conditions, insulated FRA-1-11 rosette strain gauges (Sokki Kenkyujo, Tokyo, Japan) with 120 ± 0.5 Ohm resistance were affixed to the anterior, medial, and posterior surfaces of the tibial midshaft through an incision on the medial surface, and to the anterior, medial, and lateral surfaces of the metatarsal midshaft from incisions on the medial and lateral surfaces of the leg. Gauges were sealed using M-coat and D-coat (MicroMeasurements, Inc., Raleigh, NC). To provide anesthesia and minimize inflammation, bupivacaine (diluted 1:10) was injected subcutaneously around each incision site. Muscles and tendons were retracted on the posterior and anterior surface of both bones during gauge insertion, but care was taken to ensure that these structures were not damaged. The surface of the bone at each gauge site was prepared by cutting a small window (ca. 5 mm^2) in the periosteum, cauterizing any vessels, and degreasing with 100% chloroform. Bupivacaine (diluted 1:10) was perfused under the periosteum prior to cutting, to provide anesthesia. Gauges were bonded using methyl-2-cyano-acrylate glue, with continuous pressure applied for 2 min as the glue was drying. Care was taken to ensure that one of the elements of the gauge was aligned with the long axis of the bone. The orientations of each gauge's A-element (previously marked on the gauge's sealing coat using metallic ink) relative to the long axis of the bone were recorded prior to closing the incision with suture. Gauge leads were then passed extracutaneously underneath flexible bandages to the hip, where they were sutured to a bandage loosely wrapped around the animal's abdomen. To provide strain relief, the leads of each gauge were affixed to a bandage wrapped around the leg near the site of the incision.

Strain data were recorded approximately 4 and 24 hr after surgery. Recordings were made when animals were running with an apparently normal gait and showed no signs of lameness, distress, or discomfort (e.g., with symmetrical limb kinematics on the operated and nonoperated hindlimbs, and no signs of leaning or favoring one limb over another). During each recording session, gauges were connected with insulated wire to Vishay 2120A amplifiers (MicroMeasurements, Inc., Raleigh, NC) to form one arm of a Wheatstone quarter-bridge circuit; bridge excitation was 1 V. Voltage outputs were recorded on a Teac RD-145T DAT tape recorder (Teac Corp., Tokyo, Japan). Gauges were periodically balanced to adjust for zero offsets during the experiment, and calibrated when the animal was stationary and the instrumented limb was off the ground.

To correlate strain data with limb kinematics, three-dimensional (3D) coordinates were obtained for all hindlimb joints, using a three-camera Qualisys (Qualisys, Inc., Gothenburg, Sweden) infrared 3D motion analysis system. This system tracked the position of reflective markers (12 mm in diameter) placed on the shaved skin overlying the distal inter-

phalangeal joint, distal metatarsal, lateral malleolus, lateral epicondyle of the femur, greater trochanter, and anterior superior iliac spine. Capture frequency was set at 60 Hz, and kinematic sequences were synchronized to output from the strain gauges, using a trigger that started data capture by the Qualysis system at the same time that a 2-V pulse signal was sent to the tape recorder. Limb segments were identified by connecting adjacent markers. QTools software (Qualisys, Inc.) was used to identify and measure element orientation at different points in the stance cycle, including touchdown, 25% through stance phase, temporal midstance, and 75% through stance phase.

Strain analysis

Selected sequences of strain data were sampled from the tape recorder on a Macintosh G4 computer, using an Ionet™ A-D board (GW Instruments, Somerville MA) at 250 Hz. A Superscope 3.0™ (GW Instruments) virtual instrument (written by D.E.L.) was used to determine the zero offset, calculate strains (in microstrain units ($\mu\epsilon$) of principal tension (ϵ_1) and compression (ϵ_2) from raw voltage data using shunt calibration signals recorded during the experiments, and calculate the orientation of principal tension in degrees relative to the axis of the long axis of the limb (ϵ_1), using formulae from Biewener (1992). In addition, a Mohr's circle analysis was used to calculate the magnitude of strain normal to the cross section (ϵ_y) for each gauge, following formulae in Hibbeler (1999). Igor Pro version 3.01 (Wavemetrics, Inc., Lake Oswego, OR) was used to analyze strain data from different points in the stance cycle (see above) for at least 10 stance phases per animal.

To characterize midshaft strain environment, digitized transverse cross sections of each bone midshaft were analyzed with an NIH Image macro (written by S. Martin, University of Melbourne) to calculate and graph the neutral axis and gradients of normal strain across the section, using a beam analysis model (formulae in Rybicki et al., 1974; Biewener, 1992; Gross et al., 1992). The macro solves three linear equations:

$$\varepsilon_1 = ax_1 + by_1 + c$$

$$\varepsilon_2 = ax_2 + by_2 + c$$

$$\varepsilon_3 = ax_3 + by_3 + c$$

where ϵ_1, ϵ_2, and ϵ_3 are the normal strains recorded at three sites on the bone cortex with the coordinates (x_1, y_1), (x_2, y_2), and (x_3, y_3), and a, b, and c are constants. The longitudinal normal strains measured by the three strain gauges (ϵ_1 through ϵ_3) and their respective coordinate locations ($x_{1–3}$, $y_{1–3}$) are used to solve for the three unknown parameters. The equation defining any strain isocline, ϵ_i, including the neutral axis (where $\epsilon_i = 0$), can then be solved as:

$$\varepsilon_i = ax + by + c,$$

and x and y coordinates of points on the neutral axis can be calculated using this equation.

It is not possible to calculate error for strain gauge isoclines. However, strain gauges provide highly accurate and precise data when they are bonded tightly to the bone surface and calibrated properly (for discussion, see Biewener, 1992). Slight errors most commonly occur from temporal fluctuations in the balance of the Wheatstone quarter bridges, and from inaccurate measurements of the position of the gauges on the midshaft cross section or the orientation of the gauge's elements relative to the long axis of the bone. Gauge positions and orientations, however, were measured ex vivo. In addition (as noted above), gauges were frequently balanced during the experiment, with adjustments typically less than 5 mV (1 mV is equivalent to about 1$\mu\epsilon$).

Morphological measurements

Following euthanasia of animals used in strain gauge analysis, the hindlimbs were dissected, and the orientation of each gauge was recorded. In all animals, biarticular lengths of the femur, tibia, and metatarsal were measured using digital calipers. Femoral length was measured from the most proximal point on the femoral head to the line connecting the two distal condyles; tibial length was measured from the center of the lateral condylar surface to the center of the distal articular surface; metatarsal length was measured from the center of the proximal articular surface to the most distal point of the distal articular surface. A 1-cm section was then cut from the midshaft of the tibia and metatarsal at the level of the gauges, and photographed using a digital camera on 1-mm graph paper.

SMA calculations

Cross-sectional properties were calculated in two ways. First, an NIH Image version 1.61 (http://rsb.info.nih.gov/nih-image/) macro written by M. Warfel (Cornell University) was used to calculate SMAs, using the assumption that the NA runs through the area centroid of each cross section. The macro works by calculating the coordinates of the area centroid, and then calculating I as the sum of the areas of each pixel times their squared distances to defined axes that pass through the centroid. I_{xx} and I_{yy} are area moments calculated around centroidal axes (CA) in the mediolateral (CA_{xx}) and anteroposterior (CA_{yy}) planes; I_{max} and I_{min} are the area moments around the principal axes (CA_{max}, CA_{min}). J_c was calculated as $I_{max} + I_{min}$ (which equals $I_{xx} + I_{yy}$); and Z_c was calculated for the anteroposterior axis (following the common assumption that limb bones are bent in the sagittal plane).

Second, a different NIH macro (written by S. Martin, University of Melbourne) was used to calculate SMA around the experimentally determined neutral axis (see above), defined here as I_N. I_{Ny} is calculated (somewhat arbitrarily) around the axis orthogonal

TABLE 1. Tibia midstance strain data (1.5 m/sec, 10 strides)[1]

	Posterior cortex		Medial cortex		Anterior cortex	
Subject	Normal strain	ε_1 angle	Normal strain	ε_1 angle	Normal strain	ε_1 angle
616	−428.5[2] (51.3)				553.2 (60.0)	−26.8 (0.9)
574			−215.2 (46.4)	53.2 (1.6)	556.6 (100.8)	−14.8 (2.1)
562			−449.4 (71.8)	49.9 (1.3)		
539	−748.3[2] (77.9)		−312.4 (52.4)	54.4 (0.8)		
600	−759.6 (42.7)	−76.4 (0.9)	−191.7 (42.1)	50.7 (1.4)	441.4 (35.0)	−12.0 (2.0)
Grand mean	−645.5 (188.0)	−76.4 (na)	−292.2 (117.1)	52.1 (2.1)	517.1 (65.6)	−17.9 (7.9)

[1] Values in parentheses for individual subjects are standard deviations for 10 separate stance phases. Grand mean standard deviation is calculated from individual subject means.
[2] Longitudinal strain (from single element aligned with long axis).

TABLE 2. Metatarsal midstance strain data (1.5 m/sec, 10 strides)[1]

	Anterior cortex		Medial cortex		Lateral cortex	
Subject	Normal strain	ε_1 angle	Normal strain	ε_1 angle	Normal strain	ε_1 angle
574	−672.8 (37.6)	−84.4 (1.2)	−23.5 (40.5)	55 (1.9)	42.8 (29.0)	−30.9 (0.6)
539	−1,291.5[1] (36.1)		77.9 (32.5)	−35.8 (3.3)	149.8 (19.4)	−19.2 (2.5)
616	−1,124.6 (91.4)	−89.2 (0.2)	−79.4 (34.7)	73.1 (6.1)	171.6 (38.2)	−23.9 (1.0)
Grand mean	−1,029.6 (320.1)	−87.6 (4.5)	−8.4[3] (79.7)[3]	30.8[3] (58.4)[3]	121.4 (69.0)	−24.7 (5.9)

[1] Values in parentheses for individual subjects are standard deviations for 10 separate stance phases. Grand mean standard deviation is calculated from individual subject means.
[2] Longitudinal strain (from single element aligned with long axis).
[3] High standard deviations for this grand mean are a result of different gauge position relative to NA in animal 539 than in 574 and 616.

to the NA projected through the area centroid. The polar moment of area, J_N, is calculated as $I_N + I_{Ny}$. NIH Image was also used to measure the diameters of the bone in the A-P ($D_{a\text{-}p}$) and M-L ($D_{m\text{-}l}$) planes, and the perpendicular distance from the NA to the locations on the periosteal cortex of maximum tension (a_t) and compression (a_c) in the A-P plane. These measurements permit calculation of the two section moduli: Z_{Nt}, the section modulus of tension, defined as $I_N \bullet a_t^{-1}$; and Z_{Nc}, the section modulus of compression, defined as $I_N \bullet a_c^{-1}$.

RESULTS

Table 1 presents normal strains and angles at midstance for 10 typical strides at 1.5 m/sec for the tibia; Table 2 presents the same data for the metatarsal. Calculated cross-sectional distributions of strains at midstance are graphed in Figure 3. In several instances (noted in Tables 1 and 2), not all gauge elements were working, but normal strains were used from the element aligned with the long axis (no calculations of $\epsilon_1°$ are possible from these gauges). Normal strains from all metatarsal sites were available from three animals; in one metatarsal (#539), the medial gauge was located on the tensile side of the NA, whereas in the other two individuals, the medial gauge was located more caudally, on the compressive side of the NA. Unfortunately, only one animal (#600) had all tibial gauges working simultaneously. However, of the five animals studied, at least three gauges provided data from each tibial site, and results are highly comparable between individuals (Table 1). We therefore calculated mean normal strains and angles for an average tibia and for an average metatarsal, and solved for the cross-sectional distribution of strains using representative cross sections (#600 for the tibia; #539 for the metatarsal), as shown in Figure 3.

As is evident from Figure 3 and Table 1, at midstance, both the metatarsal and the tibia have higher compressive than tensile strains, which is what one would expect from a loading regime that combines bending with axial compression. Relative to the (assumed vertical) ground reaction force in the sagittal plane, the mean orientation of the tibia at midstance is 29 ± 4.5° (proximal end angled anteriorly), and the mean orientation of the metatarsal at midstance is 14 ± 2.7° (proximal end angled posteriorly). The average total strain (absolute sum of strain on the anterior and posterior cortices) at midstance is 1,162 ± 122 με in the tibia, and 1,850 ± 132 με in the metatarsal. The NA is less then 10° from a mediolateral axis in both bones, and the metatarsal is bent anteriorly concave, and the tibia is bent posteriorly concave.

The orientation of principal tensile strains measured at gauges on the cortices at midstance corresponds reasonably well to a regime of bending. In bending, $\epsilon_1°$ of gauges on cortices subject to net tension should be aligned with the long axis of the bone, and $\epsilon_1°$ of gauges on cortices subject to net compression should be perpendicular to the long axis of the bone. As Table 1 indicates, maximum principal strains on the posterior and anterior cortices of the tibia are mostly aligned within 20° of expected orientations (the anterior maximum principal strain is predicted to be 0°, and the posterior maximum principal strain is predicted to be 90°,

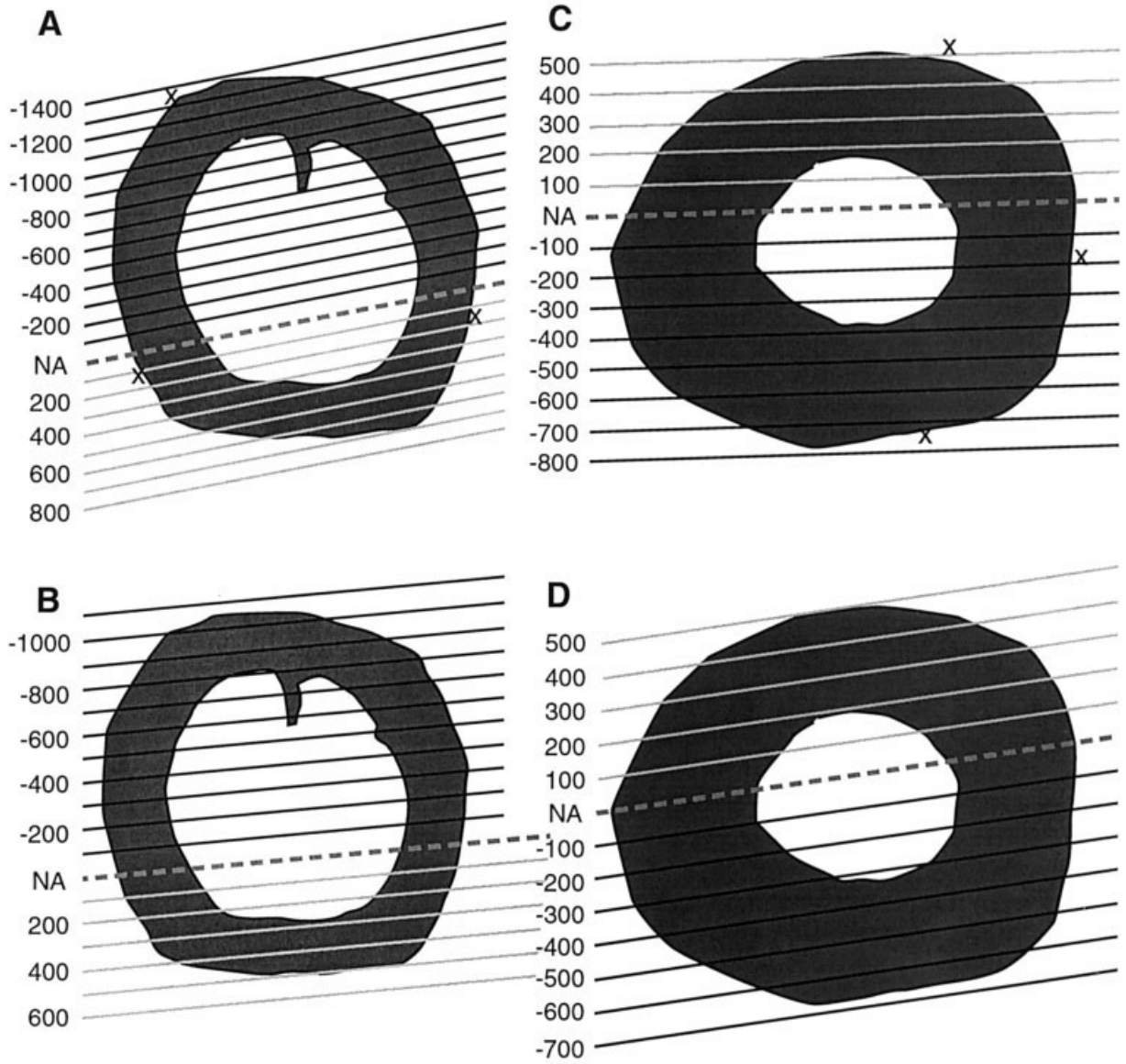

Fig. 3. Strain distribution in midshaft cross sections of sheep metatarsal and tibia at midstance at 1.5 m/sec. In all midshafts, anterior (cranial) is at top, and lateral is to left. **A:** Metatarsal sheep 539. **B:** Mean metatarsal (calculated from Table 2). **C:** Tibia sheep 600. **D:** Mean metatarsal (calculated from grand means in Table 1). NA, neutral axis. Tensile strains are positive; compressive strains are negative. X, location of strain gauges (not shown for B and D).

relative to the long axis of the bone). Similarly, the maximum principal strain orientation on the anterior cortex of the metatarsal is within 10° of the expected 90°. Principal strain trajectories cross the neutral axis of bending at 45° angles, and principal strains on the lateral and medial cortices should therefore be close to this angle. The angle on the medial cortex of the tibia is within 10° of this value (Table 1). The angles on the medial and lateral cortices of the metatarsal are more variable (Table 2), which may reflect less consistency in gauge position relative to the neutral axis of bending.

Figures 4 and 5 illustrate the cross-sectional distribution of strains at different times during the stance phase for the tibia and metatarsal. Figures 4 and 5 show that midstance is reasonably representative of strains at 25% through stance, but substantially different from the cross-sectional distribution of strains shortly after touchdown and at 75% through the stance phase. In particular, there is a counterclockwise rotation and caudal migration of the NA in both the tibia and the metatarsal between touchdown and 75% of stance. In the tibia, the NA rotates about 65°; in the metatarsal, the NA rotates about 40°. In addition, as one would expect, strains in both bones are quite low at touchdown, rise quickly, and then decline again after midstance.

Figure 6 compares the orientations of the experimentally determined neutral axes of bending with the orientation of the principal centroidal axes around which the cross sections offer the greatest and smallest resistance in bending in the three

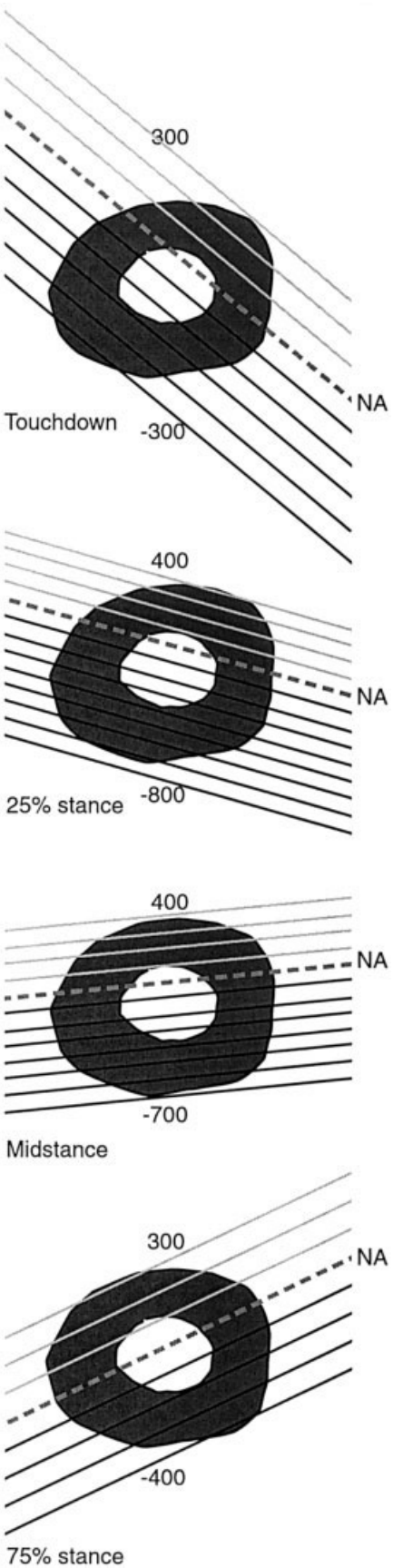

Fig. 4. Strain isoclines in 100-με intervals in tibia of sheep 600 at 1.5 m/sec at different points during stance phase. NA, neutral axis. Anterior (cranial) is at top; lateral is to left.

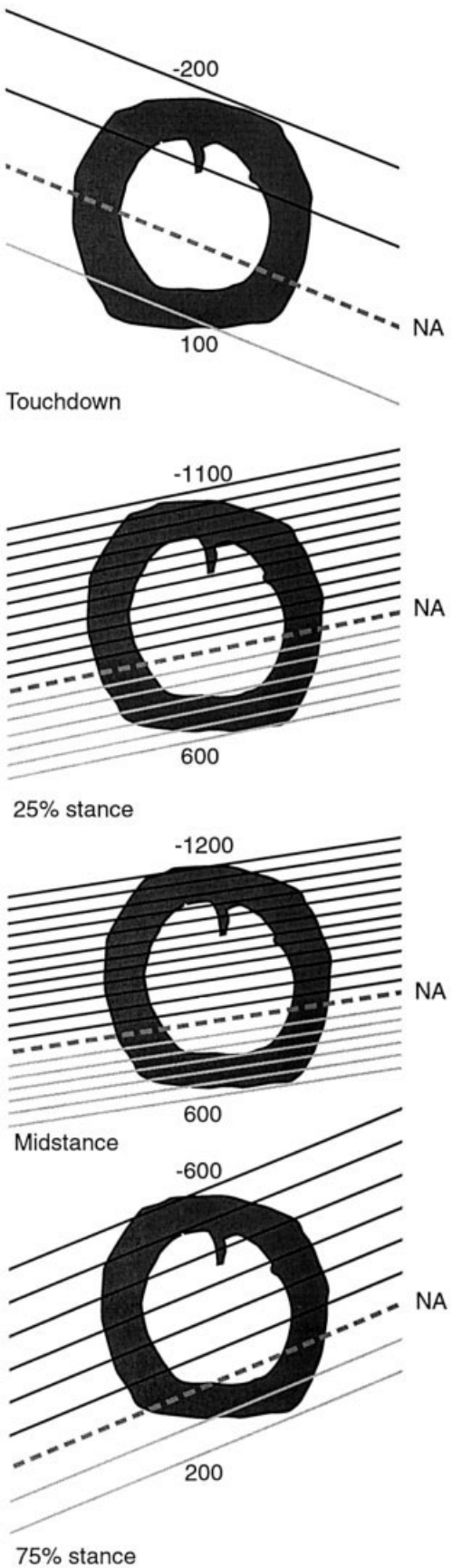

Fig. 5. Strain isoclines in 100-με intervals in metatarsal of sheep 539 at 1.5 m/sec at different points during stance phase. NA, neutral axis. Anterior (cranial) is at top; lateral is to left.

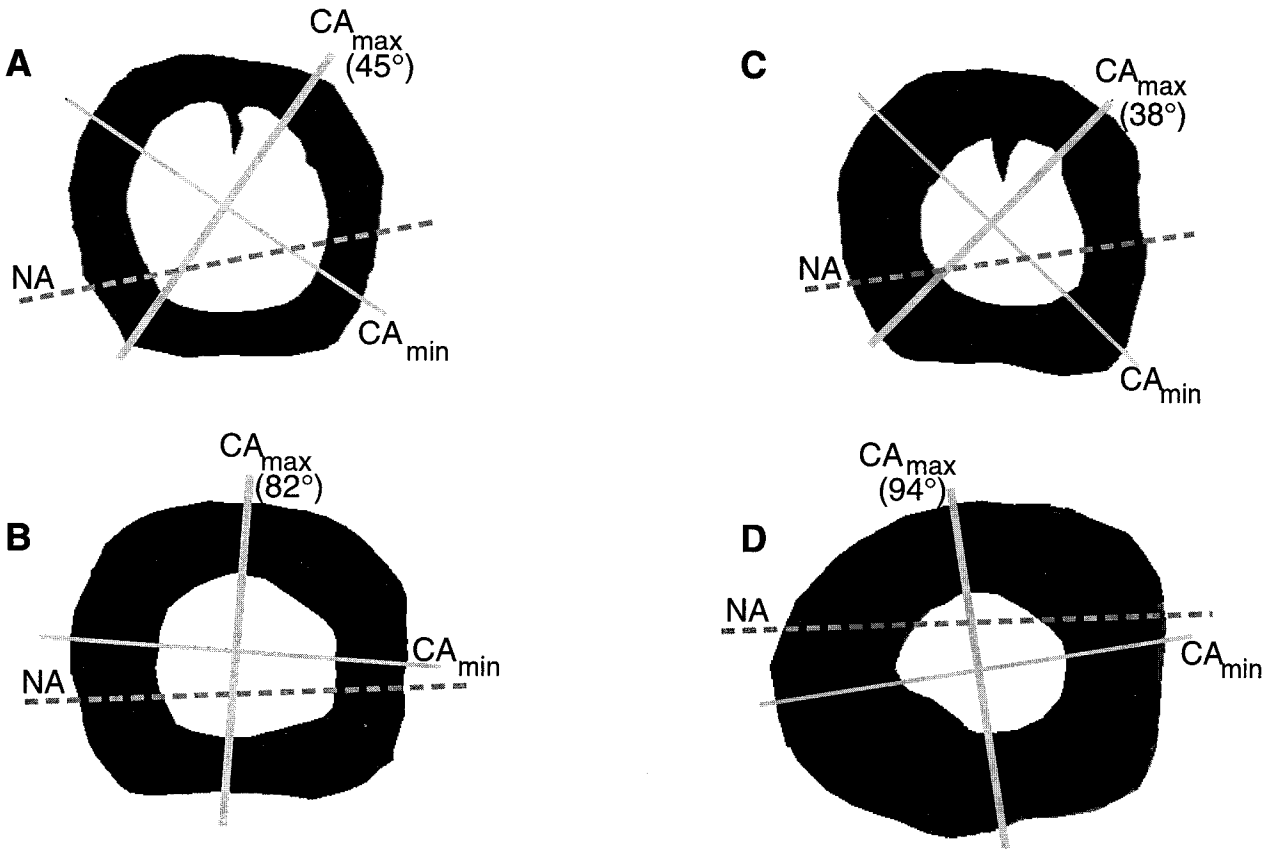

Fig. 6. Orientation of neutral axis of bending (NA) calculated at midstance at 1.5 m/sec from strain data relative to orientation of principal centroidal axes (CA_{max} and CA_{min}) around which cross section offers greatest resistance to bending relative to NA. Anterior (cranial) is at top; lateral is to left. **A:** Sheep 539 metatarsal. **B:** Sheep 574 metatarsal. **C:** Sheep 616 metatarsal. **D:** Sheep 600 tibia.

TABLE 3. Cross-sectional properties (CSPs) calculated around experimentally determined neutral axes vs. centroidal axes (% difference in parentheses)[1]

	CSPs around experimentally determined NAs								CSPs (around axis through centroid)						
Individual (bone)	I_N	I_{Ny}	J_N	Z_{Nc}	Z_{Nt}	I_N/I_{Ny}	a_t/a_c	*Theta*[2]	I_{xx}	I_{yy}	I_{max}	I_{min}	J_C	Z_C	I_{xx}/I_{yy}
539 (metatarsal)	1,025.3	768.6	1,793.9	130.3	275.6	1.3	2.1	9	738.8 (28)	760	777.4	720.9	1,498.3 (16)	65.4 (50)	1.0 (23)
574 (metatarsal)	1,001.9	951.8	1,953.7	143.7	300	1.1	2.1	4	732.8 (27)	949	950.7	731.5	1,682.2 (14)	71.1 (51)	0.8 (27)
616 (metatarsal)	1,234.3	828.7	2,063	158.2	322.3	1.5	2	8	760.4 (38)	764	823.4	701.4	1,524.7 (26)	70.4 (55)	1.0 (33)
600 (tibia)	1,415.3	1,594.0	3,009.5	192.6	345.2	0.9	1.8	3	1,093.1 (23)	1,594	1,606.5	1,080.0	2,686.7 (11)	95.5 (50)	0.7 (22)

[1] Difference = (CSP calculated from centroidal axis − CSP calculated from NA)*100. I_N, SMA around experimentally determined NA; I_{Ny}, SMA perpendicular to experimentally determined NA, through area centroid; J_N, polar moment of area based on experimentally determined axes (I_N, + I_{Ny}); Z_{Nc}, section modulus of compression around experimentally determined NA; Z_N, section modulus of tension around experimentally determined NA; a_c/a_c, ratio of distance from experimentally determined NA to cortices subject to tension (a_t) and compression (a_c); I_{xx}, SMA around mediolateral axis through centroid; I_{yy}, SMA around anteroposterior axis through centroid; I_{max}, maximum SMA around a centroidal axis; I_{min}, minimum SMA around a centroidal axis (perpendicular to I_{max}); J_c, centroidal polar moment of area (I_{xx} + I_{yy}); Z_c, centroidal section modulus. See text for further details.
[2] I_N° counterlockwise from horizontal or mediolateral (I_{xx}).

metatarsals and one tibia for which a complete set of strain data was available (see Table 1). Table 3 summarizes cross-sectional properties, and differences between area properties calculated using the experimentally determined bending axes and the centroidal axes determined solely from the geometry of the cross sections. These results show that the metatarsal and tibia are subjected primarily to bending in near-sagittal planes (the angle of the neutral axis of bending relative to the mediolateral plane, ∅, is less than 10° for all midshafts at midstance). The NA at midstance does not run through the centroid (indicated by the intersection of the CA_{max} and CA_{min} axes) of either the metatarsal or the tibia, but is shifted about two-thirds of the way towards the caudal (posterior) cortex in the metatarsal, and about two-thirds of the way towards the cranial (anterior) cortex in the tibia, most likely due to the superimposition of axial compression on a bending regime (see above).

The orientation of the neutral axis does not correspond with the maximum principal centroidal axis

TABLE 4. Least square regression of logged cross-sectional properties calculated using estimated NA vs. CA

Independent variable[1]	Dependent variable[2]	N	Bone	Slope	Slope 95% confidence interval	Intercept	Intercept 95% confidence interval	r
I_N	I_{xx}	30	Metatarsal	0.98	0.87–1.09	−0.13	−0.97–0.71	0.94
I_N	I_{xx}	30	Tibia	1.06	0.91–1.21	−0.70	−1.88–0.45	0.94
Z_{Nt}	Z_c	30	Metatarsal	0.94	0.80–1.08	2.12	1.27–2.98	0.91
Z_{Nt}	Z_c	30	Tibia	0.99	0.79–1.20	0.95	−1.09–1.28	0.87
Z_{Nc}	Z_c	30	Metatarsal	0.94	0.80–1.08	2.62	1.84–3.41	0.91
Z_{Nc}	Z_c	30	Tibia	0.99	0.79–1.20	−0.65	−2.00–0.69	0.87
J_N	J_c	30	Metatarsal	1.02	0.96–1.08	−0.27	−0.76–0.21	0.99
J_N	J_c	30	Tibia	1.05	0.99–1.12	−0.58	−1.16–0.10	0.98

[1] Calculated using NA derived from a_t/a_c from Table 3.
[2] Calculated using CA.

of the midshaft cross sections. Instead, it falls close to the minimum principal centroidal axis of the tibia cross section, and runs at approximately 45° angles to the centroidal axis of the metatarsal cross sections (Fig. 6). I_{max} therefore does not predict the plane of bending at midstance. Because of the roughly tubular shape of the metatarsal, absolute values of I_{max} and I_{min} are fairly similar in magnitude, but orientations of CA_{max} (around which I_{max} is calculated) are between 38–45° from the observed plane of bending (NA). In the tibia, the nearly A-P orientation of CA_{max} indicates that the midshaft is strongest at resisting mediolateral bending, and CA_{max} thus is nearly perpendicular to the experimentally determined NA.

Because of the differences between principal centroidal axes and experimentallydetermined neutral axes, calculations of I_{xx} in which the NA passes through the centroid and runs strictly mediolaterally are highly inaccurate in terms of their absolute value relative to I_N (the second moment of area calculated around the experimentally determined neutral axis), ranging in error from 23–38% (Table 3). Values of J are better (differences range from 11–26%), but it should be noted that I_{Ny} (which contributes to J_N) was calculated somewhat arbitrarily by assuming that the NA passed through the centroid, perpendicular to I_N. This assumption in calculating I_{Ny} reduces errors in J depending on ∅, the orientation of I_N relative to the mediolateral axis. As ∅ approaches 0°, I_{Ny} and I_{yy} will be identical. Finally, values of Z (section moduli) are extremely divergent, depending on whether they were calculated using NA vs. CA (differences can be up to 55%), because errors in the second moments of area are magnified by the inclusion of distances from the NA to the outer cortices of compression and tension (a_c, a_t). As Table 3 shows, the ratio of a_t/a_c is about 2.0 in the metatarsals and 1.8 in the tibia, both different from 1.0, the value this ratio assumes when Z is calculated around a centroidal axis.

Finally, Table 4 compares the slopes and intercepts of regressions for logged values of I, J, and Z in a large sample of juvenile, subadult, and adult sheep in which these parameters were calculated using the area centroid (I_{xx}, J_c, and Z_c) as well as the average position of the NA relative to the anterior and posterior cortices (a_t/a_c from Table 3) from the strain-gauged animals (I_N, J_N, Z_{Nc}, and Z_{Nt}). We caution that these regressions involve several assumptions, most notably that the position of NA determined in the small sample of strain-gauged sheep (summarized in Table 3) can be used to estimate the position of NA in a larger sample of sheep, most of which are older. This assumption needs to be tested. In addition, because we calculate NA position from the mean ratio of a_t/a_c, we are calculating cross-sectional properties using an anatomical plane rather than experimental bending planes, which probably vary in location between individuals. Thus correlations between the two ways of calculating cross-sectional properties are undoubtedly inflated. With these caveats in mind, the correlations between logged cross-sectional properties calculated using CAs vs. NAs are high, with no slopes that differ significantly from 1.0, but with widely varying intercepts. As one would predict, calculations of cross-sectional properties using CAs underestimate to different degrees the values based on experimentally derived estimates of NA position.

DISCUSSION

The results of this study lend support to previous models of limb-loading that predict or show long bone midshafts to be strained by a combination of bending and axial compression, with the neutral axes of bending displaced towards the cortex subject to tension (e.g., Pauwels, 1948; Lovejoy et al., 1976; Biewener et al., 1983, 1988; Rubin and Lanyon, 1982; Biewener and Taylor, 1986, Gautier et al., 2000; Gies and Carter, 1982; Gross et al., 1992). In the sheep metatarsals and tibiae studied here, compressive strains are higher than tensile strains on opposing anterior and posterior midshaft cortices, with NAs shifted away from the centroid and towards the cortex, subject to tension in both midshafts. The angles of principal tensile strains relative to the long axes of the bones also suggest that bending is the predominant loading regime to which the bones were subjected.

The first hypothesis (that cross-sectional geometric properties calculated around an experimentally determined NA are equal to or approximate those calculated through the CA) is rejected in this study.

Because most estimates of bending rigidity (I, J, and Z) depend on the squared distance of unit areas from NA, slight deviations in the position and orientation of the neutral axis relative to the centroidal axis will have large effects on the absolute values of cross-sectional properties. Thus, the shift in NA position relative to the centroid, along with differences in NA orientation relative to the orientation of I_{max} documented in the sheep tibia and metatarsal, introduce substantial differences between cross-sectional geometric properties calculated using CA vs. NA (Table 3). Differences in I range from 23–38%. Estimates of Z in the anteroposterior plane have even higher differences (50–55%), because they compound differences in I_x along with errors in the bending moment arm (assumed to be half the diameter of the bone in the plane of bending). Differences in J ($I_N + I_{Ny}$ compared to $I_{xx} + I_{yy}$) are somewhat lower (11–26%), largely because the way in which we calculated I_{Ny} gives broadly comparable results to I_{yy}, assuming NA to run through the cross-sectional centroid. Finally, descriptors of cross-sectional shape ($I_x \bullet I_y^{-1}$ vs. $I_N \bullet I_{Ny}^{-1}$) also have large differences (23–33%).

While the *absolute* value of cross-sectional properties such as I, J, and Z tends to be quite different from the value of the same parameters calculated from experimentally determined NA position, the *pattern* of differences between the two sets of parameters is highly correlated. As shown in Table 4, when data on midstance NA position from strain-gauged animals are extrapolated to a larger sample, the correlations between logged cross-sectional parameters measured using NAs vs. CAs are high ($r^2 \geq 0.87$), and none differ significantly from 1.0. Cross-sectional parameters calculated using CAs tend to underestimate the same parameters calculated using NAs, but to different degrees. Further research from a larger sample is necessary to evaluate more completely the relationship between cross-sectional geometric properties determined using centroidal vs. experimentally determined NAs.

The second hypothesis tested here (that the NA coincides in its orientation with the principal, centroidal axis of the cross section, i.e., CA_{max}, the axis around which the cross section offers greatest resistance to bending) is also rejected. As documented here, the tibia and metatarsal are predominantly bent in sagittal planes around mediolateral neutral axes at midstance, yet the maximum resistance to bending is offered in diagonal or mediolateral planes for the metatarsal and tibia, respectively. These results corroborate some previously reported experimental studies of cross-sectional strains and cross-sectional geometry in mammals and birds, which found that bones were not necessarily most reinforced structurally in the direction in which peak bending strains occur (Rubin, 1984; Gross et al., 1992; Cubo and Casinos, 1998), and that the orientation of CA_{max} does not necessarily correspond with experimentally determined directions of peak bone bending during all locomotor activities (Demes et al., 1998, 2001). Midshaft cross-sectional shapes of limbs therefore do not necessarily reflect habitual loading patterns during locomotion in the same ways in all animals.

Variations in bone design as well as speed and gait certainly complicate any effort to interpret the relationship between orientations of peak bending and cross-sectional geometric properties. As noted above, one study (Szivek et al., 1992) found the canine femur to be subjected to higher anteroposterior bending at faster speeds, which appears to correlate with the slightly anteroposteriorly elongated shape of the femoral midshaft. The one other study that explicitly compared midshaft strains in walking and galloping macaques to midshaft cross-sectional shape found a slightly improved correspondence between the orientations of CA_{max} and NA at higher speeds for the tibia, but not the ulna (Demes et al., 1998, 2001). These contrasting results are hard to interpret, and more experimental data are required to understand the relationship between bone loading and cross-sectional shape. One hypothesis is that distal bone midshafts are optimized to resist more variable loading patterns because they tend to have lower safety factors. For example, in the sheep studied here, the metatarsals are approximately tubular, causing the bones to have similar resistance to bending in most axes (I_{max} and I_{min} are almost equal). However, the same explanation does not apply to the horse third metacarpal, whose wide shape gives it greatest strength around an anteroposterior axis in spite of huge strains ($-2{,}400$ $\mu\epsilon$ of compression, and 610 $\mu\epsilon$ of tension) around a mediolateral axis (Gross et al., 1992). Accordingly, some researchers suggest that certain bones sacrifice strength in particular planes order to increase the predictability of loads in response to a variety of loading conditions (Lanyon, 1984; Bertram and Biewener, 1988), a problem that may be especially important in distal elements. Alternatively or additionally, midshaft bone shape may reflect constraints on muscle attachments. In the case of the sheep tibia, the wide shape may have little to do with resistance to bending, but instead results from the need to accommodate a sufficiently large surface area for the origins of the major ankle flexors and extensors. More experimental data are needed to test these hypotheses, but on the basis of the available evidence, it is most sensible to conclude that cross-sectional properties may not provide reliable information about patterns or magnitudes of habitual loading. Consequently, we caution against attempts to infer habitual patterns of loading based on analyses of cross-sectional geometry (including $I_{max} \bullet I_{min}^{-1}$) in the absence of experimental data for the bone and species in question.

The third hypothesis tested here (that the orientation and position of NA during the stance phase are stable and similar to its position during midstance) is partially rejected. During stance phase in the sheep, there is a substantial rotation (40–65°)

along with a slight posterior translation of the NA in both the metatarsal and tibia. As noted above, these findings indicate more change in NA position than reported in other studies on the horse metacarpal (Gross et al., 1992), the dog femur (Szivek et al., 1992), and the macaque ulna and tibia (Demes et al., 1998, 2001). Therefore, NA position may be more variable than previously hypothesized, depending on element and species. However, in terms of the magnitude of bending strains across stance, the results of this study are consistent with other studies. In the sheep, strain magnitudes are low at touchdown, reach near peak levels at 25% through stance phase, peak at midstance, and then decline substantially by 75% through stance phase. Consequently, the magnitude and orientation of loading at the midshaft are somewhat dynamic, but consistent through that part of stance when strains are high. The forces that cause these changes need to be studied but probably include shifts in the orientation of the ground and joint reaction forces relative to limb segment orientation, combined with changes in muscle activity.

We therefore conclude that cross-sectional properties estimated using centroidal axes have two major problems that need to be considered explicitly when applied to humans and other species in which in vivo strain data are not available. First, while it has long been appreciated the superimposition of bending and axial compression shifts NA away from the cross-sectional area centroid of most bones, the effect of this shift on quantitative estimates of bone strength had not been previously measured. Our study shows that calculations of cross-sectional resistance to bending around a centroidal axis differ substantially in absolute value from calculations of the actual cross-sectional resistance to bending in a bone around the neutral axis. Second, the results of this study suggest that there is no consistent and predictable relationship between the shape of a bone midshaft and the nature of the loading regime it encounters.

Before we turn to the implications of these findings for comparative studies of cross-sectional geometry in humans and other mammals, several additional issues merit discussion. Perhaps the most important is what strain gauges measure in treadmill studies vs. what bones actually experience on more normal, varied terrains. As described above, the methodology we used here calculates the position of the NA and the isoclines of strain away from the NA, based on the relative magnitude of strains normal to the midshaft cross section at three locations. Thus the pattern of relative strain between the gauges determines NA position, while the absolute magnitude of strains determines the isocline gradient. It follows that the position of NA provides information solely on how the bone is loaded, while the magnitude of strains provides information on how well the bone is counteracting the loads. Obviously, animals do not usually run on treadmills, and the nature of loads to which their limb bones are subjected is certainly much more varied in terms of the orientations of ground reaction forces, the orientations of limb elements relative to the substrate, and the force produced by different muscles. While some subtle kinematic and electromyographic differences were observed between treadmill and overground locomotion, studies on humans (Elliott and Blanksby, 1976; Scardina et al., 1985; Arsenault et al., 1986; Wank et al., 1998; Nigg et al., 1995; Alton et al., 1998; White et al., 1998) and various quadrupeds (Wetzel et al., 1975; Buchner et al., 1994; Barrey et al., 1995) show that treadmill walking and running are reasonably representative of overground gaits. However, the movement spectrum of most species exceeds the range of movements that can be elicited on a treadmill. The strains we measure on a treadmill therefore do not reflect the total range of loading patterns, but probably reflect a reasonable approximation of the typical loading pattern.

An additional issue is the limitation of sheep or any other animal model for making inferences about different animals, including humans. Sheep have many obvious differences from humans, including less muscled distal limb elements, three major long bones per limb, and gaits that are constrained to sagittal movements. But the beam model this study tested in sheep is the same as the beam model applied to humans and other species. Thus, if the application of the beam model tested here does not hold for sheep (which should be more predictable than humans), then our null hypothesis should be that the same assumptions do not hold for humans or other animals until proven otherwise.

Implications

In conclusion, we wish to highlight four major implications of these results for analyses of cross-sectional properties in the absence of strain data. First, we do not suggest that researchers abandon using cross-sectional geometry as a means of comparing bones between individuals and populations, or even between species. Analyses of cross-sectional geometry still provide better information about long bone function than simple measures of cross-sectional area. However, the results here confirm what was long suspected: that not all cross-sectional parameters are equally useful, and none are likely to be accurate in terms of absolute value. Calculations of I, J, and Z based on neutral vs. centroidal axes are highly correlated, but slopes and intercepts between the two sets of parameters will vary considerably, depending on a variety of geometrical and mechanical factors noted above. Thus, analyses that compare cross-sectional properties for the same bone within a species, or between very similar species in terms of musculoskeletal design and function (e.g., goats and sheep) where one can assume that patterns of bending are comparable, should yield results whose *patterns* are correct, but whose *absolute*

values are likely to be incorrect. For example, comparisons of midshaft J estimated from CAs in the femur between human populations (e.g., Ruff and Larsen, 1990), or between playing and nonplaying side arms of tennis players (e.g., Ruff et al., 1993, 1994), would differ from J calculated using actual NAs (whatever they may be) mostly in terms of absolute values, but the relative comparisons would probably be robust. In contrast, analyses that compare cross-sectional geometry across species with substantial differences in kinematics and anatomy (e.g., Polk et al., 2000) may be more difficult to interpret, even after standardizing by body mass and element length. While such studies often separate animals by locomotor group (e.g., Ruff and Runestad, 1992; Polk et al., 2000), more research is necessary to determine the biomechanical consequences or bases of observed differences in both absolute and relative values of cross-sectional parameters.

A second implication of these results is that J is probably the best single SMA parameter to use for analyses of cross-sectional geometry in the absence of experimental data on element loading. In typical cross sections, J provides the most accurate estimate of average bending rigidity, because errors in determination of NA position (and hence I_N) are offset by errors in the orthogonal second moment area, I_{Ny}, with the caveat that I_{Ny} errors will increase as the angle of I_x deviates from 0°. Note, however, that J is likely to produce erroneous estimates of resistance to torsion in noncircular cross sections (Wainright et al., 1976; Daegling, 2002). In addition, the section modulus, Z, is probably the worst SMA parameter to use in the absence of experimental data, because it compounds errors in I_x with errors in the distance from NA to the cortex of bending.

Third, we suggest that interpretations of function or habitual loading history based on cross-sectional shape are problematic in the absence of in vivo data on how bones are actually deformed. Evidently, and for reasons we have yet to understand, the many complex influences that contribute to bone shape pose serious challenges for efforts to interpret variations in cross-sectional geometric properties. For example, there has been a longstanding discussion about the meaning of differences in bone-shaft shape between modern humans and Neanderthals, the latter of whom typically have more bone mass distributed along the mediolateral axis of the femoral midshaft (Trinkaus, 1997; Trinkaus and Ruff, 1999; Trinkaus et al., 1999). Such differences are hard to interpret mechanically. Trinkaus (1986) suggested that the relatively wider Neanderthal midshaft might reflect more resistance to forces created by lateral movement during activities by archaic than by modern humans. In addition, Trinkaus et al. (1998a, p. 5,840) suggested that such differences in midshaft shape may be "evidence of a shift in locomotor patterns, with the presence of the femoral anteroposterior reinforcement associated with increased mobility and seen more frequently among early modern humans than among the Neandertals." However, as noted by Ruff (1995) and Trinkaus and Ruff (1999), differences in pelvic shape (Rak and Arensburg, 1987) or other anatomical factors unrelated to behavior may also contribute to the observed differences in $I_{max} \bullet I_{min}^{-1}$ between these species. We therefore agree that, at this point, it is not possible to infer reliably what, if anything, such differences in midshaft shape mean.

Finally, these data raise most clearly the problem that we need a better understanding of how bones are loaded, and the relationship between bone cross-sectional shape and both peak and habitual strains. Analyses of cross-sectional geometry do provide new insights, not possible from analyses of cross-sectional area, and we encourage their use. But the lack of any simple, predictable relationships between bone function and midshaft shape complicates interpretations of shape, and potentially invalidates comparisons between species. Further research is needed to understand better how orientations of limb elements relative to ground reaction forces and local muscle forces influence patterns and magnitudes of bone shaft loading not only during treadmill running, but also during normal activities, when variability in strain patterns will be even greater (Demes et al., 2001).

ACKNOWLEDGMENTS

We thank A. Biewener, S. Cote, M. Devlin, F. Guy, S. Martin, O. Pearson, H. Pontzer, S. Psutka, P. Ramirez, and F. Yates for technical assistance and/or helpful discussions. Useful comments were provided by the reviewers.

LITERATURE CITED

Alexander RM. 1983. On the massive legs of the Moa (*Pachyornis elephantopus*, Diornithes). J Zool Lond 202:363–376.

Alton F, Baldey, Caplan S, Morrissey MC. 1998. A kinematic comparison of overground and treadmill walking. Clin Biomech 13:434–440.

Arsenault AB, Winter DA, Marteniuk RG. 1986. Treadmill versus walkway locomotion in humans: an EMG study. Ergonomics 29:665–676.

Barnes GR, Pinder DN. 1974. In vivo tendon tension and bone strain measurement and correlation. J Biomech 7:35–42.

Barrey E, Galloux P, Valette JP, Auvinet B, Wolter R. 1993. Stride characteristics of overground versus treadmill locomotion in the saddle horse. Acta Anatomica 146:90–94.

Bertram JEA, Biewener AA. 1988. Bone curvature: sacrificing strength for load predictatibility? J Theor Biol 31:75–92.

Bertram JEA, Swartz SM. 1991. The "law of bone transformation": a case of crying Wolff? Biol Rev Cambridge Philosophic Soc 66:245–273.

Biewener AA. 1982. Bone strength in small mammals and bipedal birds: do safety factors change with body size? J Exp Biol 98:289–301.

Biewener AA. 1983. Allometry of quadrupedal locomotion: the scaling of duty factor, bone curvature and limb orientation to body size. J Exp Biol 105:147–171.

Biewener AA. 1992. In vivo measurement of bone strain and tendon force. In: Biewener AA, editor. Biomechanics—structures and systems: a practical approach. Oxford: Oxford University Press. p 123–147.

Biewener AA, Taylor CR. 1986. Bone strain: a determinant of gait and speed? J Exp Biol 123:383–400.

Biewener AA, Thomason JJ, Goodship A, Lanyon LE. 1983. Bone stress in the horse forelimb during locomotion at different gaits: a comparison of two experimental methods. J Biomech 16:565–576.

Biewener AA, Swartz SM, Bertram JEA. 1986. Bone modeling during growth: dynamic strain equilibrium in the chick tibiotarsus. Calcif Tissue Int 39:390–395.

Biewener AA, Thomason JJ, Lanyon LE. 1988. Mechanics of locomotion and jumping in the horse (*Equus*): *in vivo* stress in the tibia and metatarsus. J Zool Lond 214:547–565.

Biewener AA, Dial KP, Goslow GE Jr. 1992. Pectoralis muscle force and power output during flight in the starling. J Exp Biol 164:1–18.

Biknevicius AR. 1993. Biomechanical scaling of limb bones and differential limb use in caviomorph rodents. J Mammal 74:95–107.

Bridges PS, Blitz JH, Solano MC. 2000. Changes in long bone diaphyseal strength with horticultural intensification in west-central Illinois. Am J Phys Anthropol 112:217–238.

Buchner HHF, Savelberg HHCM, Schamhardt HC, Merkens HW, Barneveld A. 1994. Kinematics of treadmill versus overground locomotion in horses. The Veterinary Quarterly 16:S87–S90.

Burr DB, Ruff CB, Johnson C. 1989. Structural adaptation of the femur and humerus to arboreal and terrestrial environments in three species of macaque. Am J Phys Anthropol 79: 357–367.

Carter DR, Beaupré GS. 2001. Skeletal form and function: mechanobiology of skeletal development, aging and regeneration. Cambridge: Cambridge University Press.

Carter DR, Vasu R, Spengler DM, Dueland RT. 1981. Stress fields in the unplated and plated canine femur from *in vivo* strain measurements. J Biomech 14:63–70.

Churchill SE, Smith FH. 2000. A modern human humerus from the early Aurignacian of Vogelherdhöhle (Stetten, Germany). Am J Phys Anthropol 112:251–273.

Cubo J, Casinos A. 1998. Biomechanical significance of cross-sectional geometry of avian long bones. Eur J Morphol 36:19–28.

Daegling DJ. 2002. Estimation of torsional rigidity in primate long bones. J Hum Evol 42:229–239.

Demes B, Jungers WL. 1989. Functional differentiation of long bones in lorises. Folia Primatol (Basel) 52:58–69.

Demes B, Jungers WL. 1993. Long bone cross-sectional dimensions, locomotor adaptations, and body size in prosimian primates. J Hum Evol 25:57–74.

Demes B, Jungers WL, Selpien K. 1991. Body size, locomotion and long bone cross sectional geometry in Indriid primates. Am J Phys Anthropol 86:537–547.

Demes B, Stern JT, Hausman MR, Larson SG, McLeod KJ, Rubin CT. 1998. Patterns of strain in the macaque ulna during functional activity. Am J Phys Anthropol 106:87–100.

Demes B, Qin YX, Stern JT, Larson SG, Rubin CT. 2001. Patterns of strain in the macaque tibia during functional activity. Am J Phys Anthropol116:257–265.

Dial KP, Biewener AA. 1993. Pectoralis muscle force and power output during different modes of flight in pigeons (*Columba livia*). J Exp Biol 134:1–16.

Elliott BC, Blanksby BA. 1976. A cinematographic analysis of overground and treadmill running by males and females. Med Sci Sports 8:84–87.

Gautier E, Perren SM, Cordey J. 2000. Strain distribution in plated and unplated sheep tibiae. An in vivo experiment. Injury [Suppl] 31:37–44.

Gies AA, Carter DR. 1982. Experimental determination of whole long bone sectional properties. J Biomech 15:297–303.

Goodship AE, Cunningham JL. 2001. Pathophysiology of functional adaptation of bone in remodeling and repair in vivo. In: Cowin SC, editor. Bone mechanics handbook. Boca Raton: CRC Press, pp. 26–31.

Gross TS, McLeod KJ, Rubin CT. 1992. Characterizing bone strain distributions in vivo using three triple rosette strain gages. J Biomech 25:1081–1087.

Gross TS, Edwards JL, McLeod KJ, Rubin CT. 1997. Strain gradients correlate with sites of periosteal bone formation. J Bone Miner Res 6:982–988.

Heinrich RE, Rose KD. 1997. Postcranial morphology and locomotor behavior of two early Eocene miacoid carnivorans, *Vulvapus* and *Didymictis*. Palaeontology 40:279–305.

Heinrich RE, Ruff CB, Adamczewski JZ. 1999. Ontogenetic changes in mineralization and bone geometry in the femur of muskoxen (*Ovibos moschatus*). J Zool Lond 247:215–223.

Hibbeler RC. 1999. Mechanics of materials, 4th ed. Upper Saddle River, NJ: Prentice Hall.

Judex S, Gross TS, Zernicke RF. 1997. Strain gradients correlate with sites of exercise-induced bone-forming surfaces in the adult skeleton. J Bone Miner Res 12:1737–1745.

Jungers WL, Burr DB. 1994. Body size, long bone geometry and locomotion in quadrupedal monkeys. Z Morphol Anthropol 80: 89–97.

Jungers WL, Burr DB, Cole MS. 1998. Body size and scaling of long bone geometry, bone strength and positional behavior in cercopithecoid primates. In: Strasser E, Fleagle JG, Rosenberger A, McHenry H, editors. Primate locomotion: recent advances. New York: Plenum Press. p 309–330.

Kimura T. 2002. Primate limb bones and locomotor types in arboreal or terrestrial environments. Z Morphol Anthropol 83: 201–219.

Lanyon LE, Rubin CT. 1985. Functional adaptation in skeletal structures. In:

Hildebrand M, Bramble DM, Liem KF, Wake DB, editors. Functional vertebrate morphology. Cambridge, MA: Harvard University Press. p 1–25.

Lieberman DE. 1996. How and why humans grow thin skulls: experimental evidence for systemic cortical robusticity. Am J Phys Anthropol 101:217–236.

Lieberman DE, Pearson OM. 2001. Trade-off between modeling and remodeling responses to loading in the mammalian limb. Bull Mus Comp Zool 156:269–282.

Lieberman DE, Devlin MJ, Pearson OM. 2001. Articular area responses to mechanical loading: effects of exercise, age, and skeletal location. Am J Phys Anthropol 116:266–277.

Llorens L, Casinos A, Berge C, Majoral M, Jouffroy FK. 2001. A biomechanical study of the long bones in platyrrhines. Folia Primatol (Basel) 72:201–216.

Lovejoy CO, Burstein AH, Heiple KG. 1976. The biomechanical analysis of bone strength: a method and its application to platycnemia. Am J Phys Anthropol 44:489–505.

Martin RB, Burr DB, Sharkey N. 1999. Skeletal tissue mechanics. New York: Springer.

Nigg BM, De Boer RW, Fisher V. 1995. A kinematic comparison of overground and treadmill running. Med Sci Sports Exerc 27:98–105.

Ohman JC. 1993. Computer software for estimating cross-sectional geometric properties of long bones with concentric and eccentric elliptical models. J Hum Evol 25:217–227.

Pauwels F. 1948. Die Bedeutung der Bauprinzipien des Stütz- und Bewegungsapparates für die Beanspruchung der Röhrenknochen. Z Anat Entwickl Gesch 114:129–166.

Pearson OM. 2000. Activity, climate, and postcranial robusticity: implications for modern human origins and scenarios of adaptive change. Curr Anthropol 41:569–607.

Peterman MM, Hamel AJ, Cavanagh PR, Piazza SJ, Sharkey NJ. 2001. In vitro modeling of human tibial strains during exercise in micro-gravity. J Biomech 34:696–698.

Polk JD, Demes B, Jungers WL, Biknevicius AR, Heinrich RE, Runestad JA. 2000. A comparison of primate, carnivoran, and rodent limb bone cross-sectional properties: are primates really unique? J Hum Evol 39:297–325.

Qin Y-X, Rubin CT, McLeod KT. 1998. Nonlinear dependence of loading intensity and cycle number in the maintenance of bone mass and morphology. J Orthop Res 16:482–489.

Rak Y, Arensburg B. 1987. Kebara 2 Neanderthal pelvis: first look at a complete inlet. Am J Phys Anthropol 73:227–231.

Rubin CT. 1984. Skeletal strain and the functional significance of bone architecture. Calcif Tissue Int 36:11–18.

Rubin CT, Lanyon LE. 1982. Limb mechanics as a function of speed and gait. J Exp Biol 101:187–211.
Rubin CT, Judex S, McLeod KJ, Qin Y-X. 2001. Inhibition of osteopenia by biophysical intervention. In: Marcus R, Feldman D, Kelsey J, editors. Osteoporosis, volume 1, 2nd ed. San Diego: Academic Press. p 489–507.
Ruff CB. 1987. Structural allometry of the femur and tibia in Hominoidea and *Macaca*. Folia Primatol (Basel) 48:9–49.
Ruff CB. 1992. Biomechanical analyses of archaeological human material. In: Saunders SR, Katzenberg A, editors. The skeletal biology of past peoples. New York: Alan R. Liss. p 41–62.
Ruff CB. 1995. Biomechanics of the hip and birth in early *Homo*. Am J Phys Anthropol 98:527–574.
Ruff CB, Hayes WC. 1983. Cross-sectional geometry of Pecos Pueblo femora and tibiae—a biomechanical investigation. I. Method and general patterns of variation. Am J Phys Anthropol 60:359–381.
Ruff CB, Larsen CS. 1990. Postcranial biomechanical adaptations to subsistence changes on the Georgia coast. Anthropol Pap Am Mus Nat Hist 68:94–120.
Ruff CB, Runestad JA. 1992. Primate limb bone structural adaptations. Annu Rev Anthropol 21:407–433.
Ruff CB, Trinkaus E, Walker A, Larsen CS. 1993. Postcranial robusticity in *Homo*. I: temporal trends and mechanical interpretation. Am J Phys Anthropol 91:21–53.
Ruff CB, Walker A, Trinkaus E. 1994. Postcranial robusticity in *Homo*. III: ontogeny. Am J Phys Anthropol 93:35–54.
Runestad JA. 1997. Postcranial adaptations for climbing in Lorisidae (Primates). J Zool Lond 242:261–290.
Rybicki EF, Mills EJ. 1977. In vivo analytical studies of forces and moments in equine long bones. J Biomech 10:701–705.
Rybicki EF, Simonen FA, Mills EJ, Hassler CR, Scoles P, Milne D, Weis EB. 1974. Mathematical and experimental studies on the mechanics of plated transverse fractures. J Biomech 7:377–384.
Scardina N, Daniels J, Vanhandel P, Bradley P, Troup J. 1985. Running, cadence, stride length and respiratory frequency during treadmill and track running at sea-level and altitude. Med Sci Sports Exerc 17:249–249.
Schaffler MB, Burr DB, Jungers WL, Ruff CB. 1985. Structural and mechanical indicators of limb specialization in primates. Folia Primatol (Basel) 45:61–75.
Selker F, Carter DR. 1989. Scaling of long bone fracture strength with animal mass. J Biomech 22:1175–1183.
Stock J, Pfeiffer S. 2001. Linking structural variability in long bone diaphyses to habitual behaviors: foragers from the southern African Later Stone Age and the Andaman Islands. Am J Phys Anthropol 115:337–348.
Szivek JA, Johnson EM, Magee FP. 1992. *In vivo* strain analysis of the greyhound femoral diaphysis. J Invest Surg 5:91–108.
Terranova CJ. 1995. Leaping behaviors and the functional morphology of strepsirhine primate long bones. Folia Primatol (Basel) 65:181–201.
Trinkaus E. 1986. The Neandertals and modern human origins. Annu Rev Anthropol 15:193–218.
Trinkaus E. 1992. Morphological contrasts between the Near Eastern Qafzeh-Skhul and late archaic human sample: grounds for a behavioral difference? In: Akazawa T, Aoki K, Kimura T, editors. The evolution and dispersal of humans in Asia. Tokyo: Hokusen-Sha. p 277–294.
Trinkaus E. 1997. Appendicular robusticity and the paleobiology of modern human emergence. Proc Natl Acad Sci USA 94: 13367–13373.
Trinkaus E, Churchill SE. 1999. Diaphyseal cross-sectional geometry of Near Eastern Middle Paleolithic hominids: the humerus. J Archaeol Sci 26:173–184.
Trinkaus E, Ruff CB. 1999. Diaphyseal cross-sectional geometry of Near Eastern Middle Paleolithic hominids: the femur. J Archaeol Sci 26:409–424.
Trinkaus E, Ruff CB, Churchill SE. 1998a. Upper limb versus lower limb loading patterns among Near Eastern Middle Paleolithic hominids. In: Akazawa T, Kaoki K, Bar-Yosef O, editors. Neanderthals and modern humans in west Asia. New York: Plenum Press. p 391–404.
Trinkaus E, Ruff CB, Churchill SE, Vandermeersch B. 1998b. Locomotion and body proportions of the Sainte-Césaire 1 Châtelperonian Neandertal. Proc Natl Acad Sci USA 95:5836–5840.
Trinkaus E, Stringer CB, Ruff CB, Hennessy RJ, Roberts MB, Parfitt SA. 1999. Diaphyseal cross-sectional geometry of the Boxgrove 1 Middle Pleistocene human tibia. J Hum Evol 37:1–25.
van der Meulen MC, Beaupré GS, Carter DR. 1993. Mechanobiologic influences in long bone cross-sectional growth. Bone 14: 635–42.
Wainright SA, Biggs WD, Currey JD, Gosline JM. 1976. Mechanical design in organisms. Princeton: Princeton University Press.
Wank V, Frick U, Schmidtbleicher D. 1998. Kinematics and electromyography of lower limb muscles in overground and treadmill running. Int J Sports Med 19:455–461.
Wells RP. 1981. The projection of the ground reaction force as a predictor of internal joint moments. Bull Prosth Res 18:15–19.
Wetzel MC, Atwater AE, Wait JV, Stuart DG. 1975. Neural implications of different profiles between treadmill and overground locomotion timings in cats. J Neurophysiol 38:492–501.
White SC, Yack J, Tucker CA, Lin H-Y. 1998. Comparison of vertical ground reaction forces during overground and treadmill walking. Med Sci Sports Exerc 30:1537–1542.
Winter DA. 1990. Biomechanics and motor control of human movement, 2nd ed. New York: John Wiley & Sons.